Visualization of Hypoxia in Microscopic Tumors by Immunofluorescent Microscopy

Xiao-Feng Li, Sean Carlin, Muneyasu Urano, James Russell, C. Clifton Ling, and Joseph A. O'Donoghue

Department of Medical Physics, Memorial Sloan-Kettering Cancer Center, New York, New York

Abstract

Tumor hypoxia is commonly observed in primary solid malignancies but the hypoxic status of subclinical micrometastatic disease is largely unknown. The distribution of hypoxia in microscopic tumors was studied in animal models of disseminated peritoneal disease and intradermal (i.d.) growing tumors. Tumors derived from human colorectal adenocarcinoma cell lines HT29 and HCT-8 ranged in size from a few hundred microns to several millimeters in diameter. Hypoxia was detected by immunofluorescent visualization of pimonidazole and the hypoxia-regulated protein carbonic anhydrase 9. Tumor blood perfusion, cellular proliferation, and vascularity were visualized using Hoechst 33342, bromodeoxyuridine, and CD31 staining, respectively. In general, tumors of <1 mm diameter were intensely hypoxic, poorly perfused, and possessed little to no vasculature. Larger tumors (~1–4 mm diameter) were well perfused with widespread vasculature and were not significantly hypoxic. Patterns of hypoxia in disseminated peritoneal tumors and i.d. tumors were similar. Levels of hypoxia in microscopic peritoneal tumors were reduced by carbogen breathing. Peritoneal and i.d. tumor models are suitable for studying hypoxia in microscopic tumors. If the patterns of tumor hypoxia in human patients are similar to those observed in these animal experiments, then the efficacy of systemic treatments of micrometastatic disease may be compromised by hypoxic resistance. [Cancer Res 2007;67(16):7646–53]

Introduction

Although the existence of tumor hypoxia is a common feature of primary solid malignancies (1–5), the hypoxic status of subclinical micrometastatic disease is largely unknown. One fundamental difficulty associated with characterizing microscopic disease is the inability to localize it spatially. This, together with the existence of multiple sites of dissemination, necessitates a systemic approach to treatment, typically using chemotherapeutic drugs. It is well known that the cytotoxic effectiveness of many chemotherapeutic agents is decreased by hypoxia (6, 7). It thus follows that if hypoxic microscopic disease is present, it may be relatively resistant to treatment. Potentially, the use of a serum hypoxia marker, such as osteopontin (8, 9), may enable the existence of hypoxic subclinical disease in patients to be inferred. However, in the presence of gross disease, the incremental "signal" from micrometastases is likely to be overwhelmed.

In animal models, it is possible to observe tumor hypoxia using a variety of invasive and noninvasive means. Several studies on syngeneic or xenografted tumors in rodents using polarographic electrodes or magnetic resonance methods have indicated that smaller tumors tend to be better oxygenated than larger ones (10–12). However, the smallest tumors examined in these studies were still relatively large (~8–10 mm in diameter). Animal models of disseminated malignant disease in the lung, bone, or peritoneal cavity may be initiated by intravessel or intracavitary injection of tumor cells. Systems such as these may also be used to examine tumor hypoxia in microscopic disease but invasive methods are required, as the tumors of interest are too small (<1 mm diameter) for noninvasive imaging or probe measurements. In addition, such disseminated models generally consist of a multiplicity of individual tumors of diverse size and potentially also hypoxic status. Although this may be advantageous for some studies of tumor hypoxia, it would also be desirable to have available models of tumor hypoxia in microscopic disease that consist of single foci rather than wide dissemination to simplify assessment of the relationship between treatment and response.

The hypoxic status of microscopic tumors can be assessed by tumor sectional analysis of the distribution of exogenously administered hypoxic tracers or endogenous hypoxic markers. Pimonidazole is a 2-nitroimidazole compound that is selectively reduced and binds to intracellular macromolecules in hypoxic regions of tumors. It has been widely used in clinical and experimental studies of tumor hypoxia (13–15). Carbonic anhydrase 9 (CA9) is a hypoxia-regulated protein frequently used clinically as an endogenous marker of tumor hypoxia (16–20), although in experimental models, its level of expression varies between cell lines (21).

In this report, we describe our study of the distribution of hypoxia in microscopic tumors using a disseminated peritoneal disease model and a focal intradermal (i.d.) model in athymic mice. Tumor sizes investigated ranged in diameter from a few hundred microns to several millimeters. The presence of tumor hypoxia was detected by immunofluorescent visualization of pimonidazole and, in some instances, of the hypoxia-regulated protein CA9. Simultaneously, tumor blood perfusion, cellular proliferation, and vascularity were visualized by imaging of Hoechst 33342, bromodeoxyuridine (BrdUrd), and CD31 staining, respectively.

Materials and Methods

Tumor Cell Lines and Animals

Two human tumor cell lines were used in experiments, HT29 and HCT-8, both originally derived from colorectal adenocarcinomas. Tumor cell lines were purchased from American Type Culture Collection. HT29 and HCT-8 cells were maintained in McCoy's 5A modified medium (Life Technologies)

Note: Supplementary data for this article are available at Cancer Research Online (http://cancerres.aacrjournals.org/).

Requests for reprints: Xiao-Feng Li, Department of Medical Physics, Memorial Sloan-Kettering Cancer Center, 1275 York Avenue, New York, NY 10021. E-mail: LiX1@mskcc.org.

doi:10.1158/0008-5472.CAN-06-4353

and RPMI 1640 (Cellgro), respectively. All media were supplemented with 10% fetal bovine serum (Gemini), 1% glutamine, and 1% antibiotic mixture (Cellgro). Cells were grown at 37°C in a humidified CO_2 incubator. Exponentially growing cells were harvested with 0.05% trypsin plus EDTA for HT29 and 0.25% trypsin plus EDTA (Cellgro) for HCT-8, washed, and suspended in PBS. The number of cells was counted using a Coulter counter (Beckman Coulter).

All experiments were done using 6- to 8-week-old female athymic NCr-*nu/nu* mice purchased from National Cancer Institute-Frederick Cancer Research Institute (Bethesda, MD). Nude mice were maintained and used according to institutional guidelines. The experimental protocols were approved by the Institutional Animal Care and Use Committee. Animals were housed five per cage and kept in the institutional small animal facility at a constant temperature and humidity. Food pellets and water were provided *ad libitum*.

Establishment of Tumors in Animals

To study tumors within different size ranges, several tumor generation methods were used.

Macroscopic s.c. tumors. S.c. tumors were initiated by injecting 5×10^6 tumor cells in 0.1 mL PBS s.c. into the mouse flank. Experiments were done when tumors reached ~1 cm in average diameter, which occurred typically 3 to 4 weeks after initiation.

Microscopic peritoneal tumors. Disseminated microscopic tumors were induced in the peritoneum by injecting tumor cell suspensions ($5–10 \times 10^6$ cells/0.1–0.2 mL) into the peritoneal cavity. Animals were sacrificed typically 6 to 7 weeks (HT29) or 3 to 4 weeks (HCT-8) after tumor initiation. At this time, a distribution of tumors of varying sizes was observed to be present on or in the intestinal serosa. Tumor sizes ranged from a few hundred micrometers up to several millimeters in diameter.

Ascites tumors. At the time of sacrifice, ascites was evident in the majority of animals injected i.p. with HT29 cells. The ascites fluid was observed to be bloody and contained a distribution of free-floating tumor cell aggregates of sizes up to 1 mm in diameter, denoted here as ascites tumors. HT29 ascites tumors were typically ellipsoidal in shape with a "rough" surface and the appearance of duct-like structures in the interior. Ascites was generally not observed following i.p. injection of HCT-8 cells.

Microscopic i.d. tumors. Cell suspensions containing 2.5×10^5 (4 μL), 5×10^5 (8 μL), 10^6 (16 μL), or 2×10^6 cells (32 μL) were injected using a 100-μL syringe (Hamilton) at 4 i.d. sites per animal and allowed to grow for 3 to 7 days. Tumor sizes were dependent on the number of cells injected and the time of assay and ranged from a few hundred micrometers to several millimeters in diameter.

Exogenous Markers of Tumor Hypoxia, Perfusion, and Proliferation

Hypoxia. The hypoxic cell marker pimonidazole hydrochloride [1-[(2-hydroxy-3-piperidinyl)propyl]-2-nitroimidazole hydrochloride; 20 mg/mL in physiologic saline; 80 mg/kg; nominal injected volume, 0.1 mL; Chemicon International] was administered via tail vein injection 1 h before animal sacrifice.

Perfusion. The fluorescent dye Hoechst 33342 (5 mg/mL in physiologic saline; 15 mg/kg; nominal injected volume, 0.1 mL; Sigma-Aldrich) was administered via tail vein injection 1 min before animal sacrifice.

Proliferation. The cellular proliferation marker BrdUrd (Roche Diagnostics) first dissolved in DMSO and then in physiologic saline (20 mg/mL; 150 mg/kg; nominal injected volume, 0.19 mL) was administered via tail vein injection 1 h before animal sacrifice.

In all cases, fresh drug solutions were prepared on the day of injection.

Preparation of Frozen Tumor Sections

Immediately after animal sacrifice, tumor tissues or ascites fluid were removed for subsequent processing. S.c. and i.d. xenografts were immediately dissected, frozen on dry ice, and embedded in optimal cutting medium (OCT 4583, Sakura Finetek). Peritoneal tumors (adhering to the intestinal serosa) were washed with PBS to remove any attached ascitic tumor cells before freezing and embedding in OCT. Ascites tumors were harvested, washed with PBS to remove RBC, frozen, and embedded in OCT. For all tumor samples, sets of 10 contiguous 8-μm thick tissue sections were cut using a Microm HM500 cryostat microtome (Microm International GmbH) and adhered to poly-L-lysine–coated glass microscope slides. Frozen sections were stored at −80°C until use.

Visualization of Hypoxia, Perfusion, Proliferation, and Vasculature on Tumor Sections

To minimize issues associated with section alignment and registration, wherever possible, the same tumor section was used for all images at a given location.

Hypoxia and perfusion. Slides were air dried, fixed in cold acetone (4°C) for 20 min, and incubated with SuperBlock (Pierce Biotechnology) at room temperature for 30 min. Sections were then incubated with FITC-conjugated anti-pimonidazole monoclonal antibody (Chemicon International), diluted 1:25, for 1 h at room temperature. In some cases, HT29 tumor sections were costained for the hypoxia-regulated protein CA9 by including chimeric anti-CA9 (cG250) antibody (a gift from Dr. Gerd Ritter, Ludwig Institute for Cancer Research, New York, NY) at a final concentration of 10 μg/mL. Sections were washed three times in PBS, each wash lasting 5 min. For CA9 staining, sections were then incubated with Alexa Fluor 568–conjugated goat anti-human antibody (1:100; Molecular Probes) and washed again. Due to low expression levels, HCT-8 tumor sections were not stained for CA9.

Images were acquired at ×100 magnification using an Olympus BX40 fluorescence microscope (Olympus America, Inc.) equipped with a motorized stage (Prior Scientific Instruments Ltd.). Hoechst 33342, pimonidazole, and CA9 were imaged using blue, green, and red filters, respectively.

Proliferation. BrdUrd staining was done on HT29 sections that had been previously imaged for pimonidazole but not CA9. Sections were treated with 2 N HCl for 10 min at room temperature followed by 0.1 mol/L Borax for 10 min at room temperature. Sections were then exposed to Alexa Fluor 594–conjugated anti-BrdUrd antibody (1:20 dilution; Molecular Probes) for 1 h at room temperature and washed. Images were acquired as above using a red filter.

Vasculature. Anti-CD31 staining was done on adjacent contiguous sections to those that were stained for pimonidazole. Sections were stained for 1 h at room temperature with rat anti-mouse CD31 antibody (platelet/endothelial cell adhesion molecule 1, PharMingen) diluted 1:10 in SuperBlock and incubated at room temperature with biotinylated rabbit anti-rat IgG (Vector Laboratories) for 30 min. Subsequently, these sections were treated with Vector Elite ABC reagent (Vector Laboratories) for 30 min. Finally, color was developed by applying diaminobenzidine for 15 min. Images were acquired by light microscopy using the same system described above.

After acquisition of fluorescence images, the same tumor sections were stained with H&E and imaged by light microscopy.

To control for nonspecific binding of antibodies, stained sections were processed from similar tumors that had not been exposed to pimonidazole or BrdUrd. Controls for CD31 and CA9 staining consisted of sections where primary antibody was omitted.

Image Analysis

Analysis of spatial correspondence. The spatial correspondence between the fluorescence intensities of pimonidazole, CA9, and Hoechst 33342 was examined for the representative HT29 s.c. tumor sectional image shown in Fig. 1*A*. Briefly, a grid of squares was overlaid on the coregistered green, red, and blue fluorescence images using Metamorph 7.0 software (Molecular Devices) and fluorescence intensities in each square were recorded. A grid size of 5×5 native image pixels was selected, corresponding to squares of length 8 μm. These settings resulted in a manageable number of grid squares for the image in question ($207 \times 179 = 37{,}053$). With the aid of the corresponding H&E image, a mask was drawn around the necrotic area that was excluded from analysis. This procedure resulted in a 3-column matrix of fluorescence intensities, one column for each of pimonidazole (green), CA9 (red), and Hoechst33342 (blue) where each matrix row contained the three fluorescence intensities in individual grid squares.

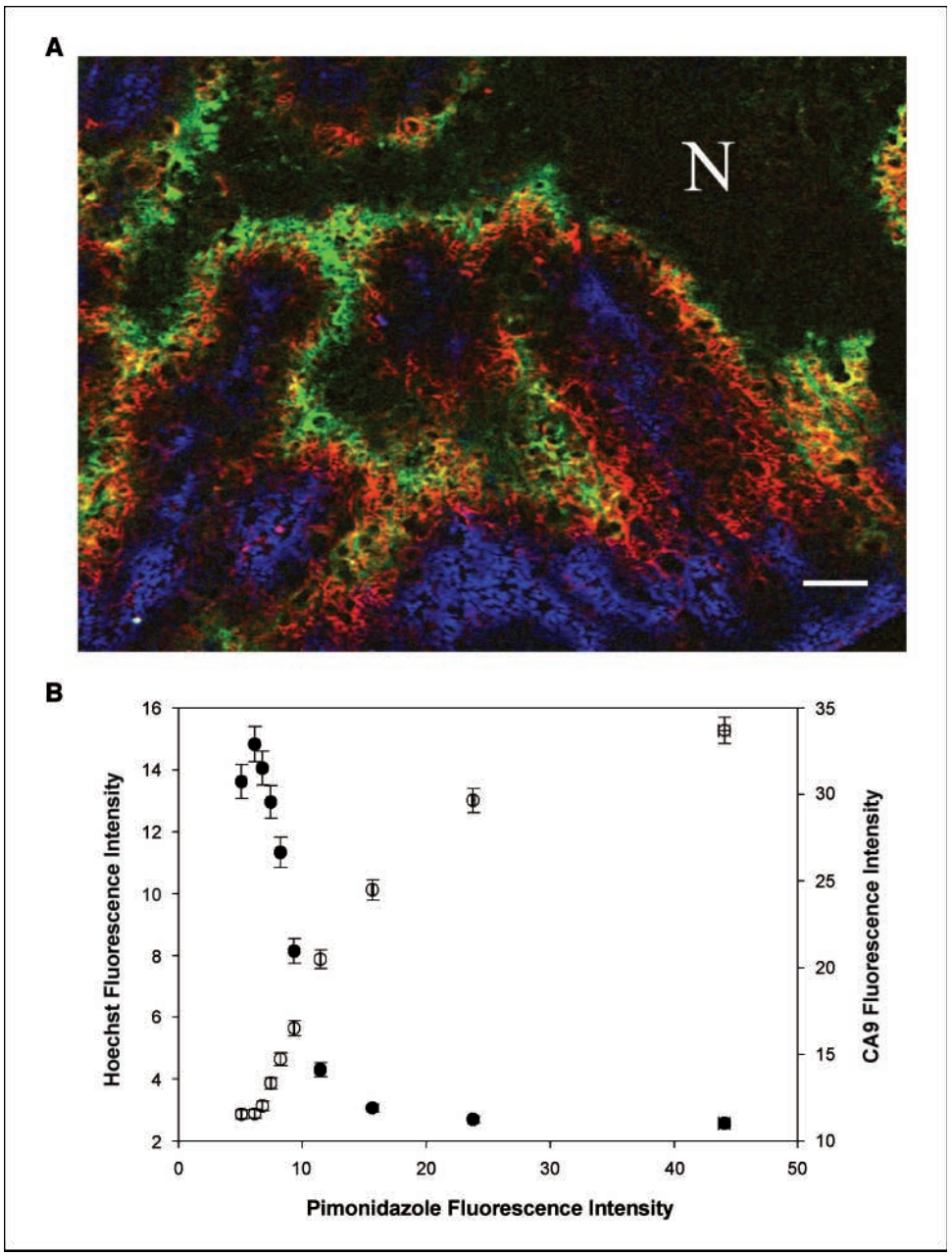

Figure 1. *A,* representative fluorescence overlay image [pimonidazole (*green*), Hoechst 33342 (*blue*), and CA9 (*red*)] of a section from a macroscopic s.c. xenograft derived from the human colorectal carcinoma cell line HT29. *N,* necrosis. *Bar*, 200 μm. *B,* the spatial correspondence between Hoechst 33342 and pimonidazole and between CA9 and pimonidazole fluorescence intensities from Fig. 1*A* (excluding areas of necrosis). The scattergram represents the decile-binned mean and 95% CIs of paired fluorescence intensity values acquired on an 8-μm square pixel-by-pixel basis. ●, Hoechst 33342 versus pimonidazole; ○, CA9 versus pimonidazole.

For comparative purposes, the data were sorted in ascending order of pimonidazole fluorescence intensity (arbitrarily selected as the independent variable). Subsequently, the data were rebinned into deciles of the independent variable (i.e., the lowest 10% of pimonidazole fluorescence intensities, then the next lowest 10%, etc.). For each bin, the mean and 95% confidence interval (95% CI) of dependent and independent variables were calculated and plotted as scattergrams.

The matrix of fluorescence intensities was also used to quantify the degree of mismatch between pimonidazole and CA9. This procedure required the use of thresholds to categorize spatial locations as either positive or negative. Thresholds were defined as a percentage of the maximum fluorescence intensity and grid squares classified as positive or negative for green or red. Grid squares were then further classified as a match (i.e., +/+ or −/−) or a mismatch (i.e., +/− or −/+). Finally, pimonidazole and CA9 thresholds were varied in tandem until the maximum mismatch was found.

Pimonidazole-positive fraction. Images were coregistered and analyzed using Adobe Photoshop 7.0. Tumor area was estimated by contouring the tumor boundary using the H&E image and the number of pixels within the boundary was converted to millimeter square. Necrotic areas were estimated in an analogous manner and subtracted from the total area to yield the viable tumor area. The pimonidazole-positive area was taken to be the millimeter square equivalent of the number of pixels that had green fluorescence intensity greater than a threshold value. The pimonidazole-positive fraction (PPF) was then defined as the ratio of pimonidazole-positive area to viable tumor area.

Thresholds for pimonidazole positivity were defined with respect to the green fluorescence intensity observed in control regions of interest (ROI). For s.c., i.d., and peritoneal tumors, control ROIs were regions within tumors where positive Hoechst 33342 fluorescence was observed. For ascites tumors, where Hoechst 33342 positivity was generally not observed, control ROIs were drawn on parts of slides that did not contain tumors.

Consistent definitions of threshold were used within each comparative study; however, alternative definitions were used for different purposes. To compare PPF for tumors of different sizes, the threshold for pimonidazole

positivity was defined as the value of green fluorescent intensity that produced a PPF of 0.5% in control ROI. In contrast, to compare PPF in tumors where hosts were breathing air or carbogen, pimonidazole positivity thresholds were defined as multiples of the mean fluorescent intensity in control ROI. These differing definitions of pimonidazole positivity threshold were selected operationally to maximize the useful range of values measured.

Carbogen Inhalation

For experiments featuring carbogen breathing, animals were placed without anesthesia in a plastic chamber of 20 × 10 × 10 cm into which carbogen (95% O_2:5% CO_2) was delivered at a flow rate of 5 L/min. After 1 h of breathing carbogen, animals were injected with pimonidazole and then returned to the carbogen chamber for another hour before Hoechst 33342 administration and sacrifice. Control animals were similarly treated but breathed room air throughout the experiment.

Experimental Logistics

The aim of these studies was to study the patterns of tumor hypoxia in the differing disease conformations. Based on the initial results, we went on to examine whether breathing carbogen influenced tumor hypoxia in peritoneal disease. The numbers of animals used in the experiments were as follows. (*a*) Hypoxia in macroscopic s.c. tumors was studied in five animals each for HT29 and HCT-8 xenografts with one tumor per animal. (*b*) Hypoxia in disseminated peritoneal tumors was studied in nine animals each for HT29 and HCT-8, each animal having a distribution of tumors of

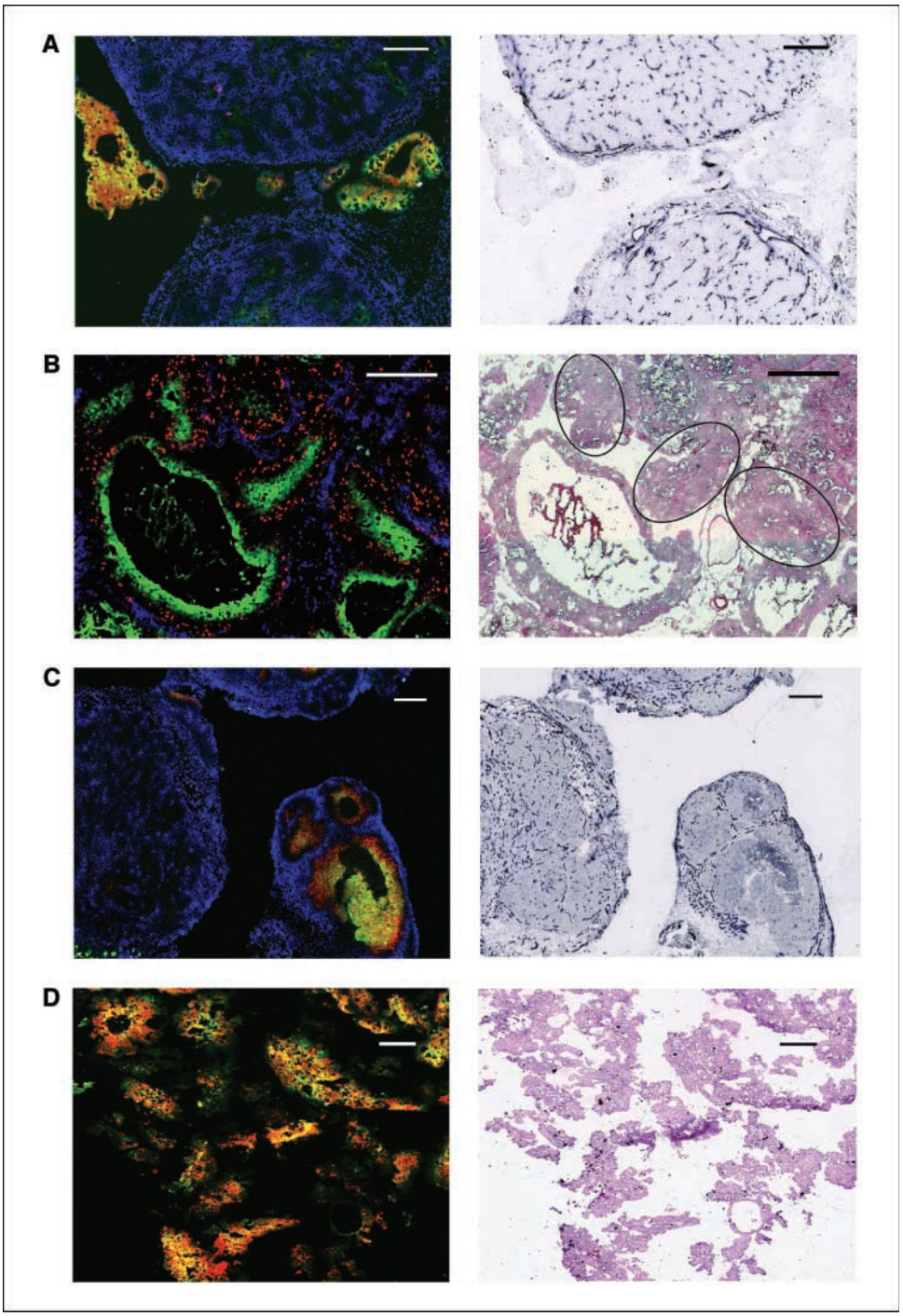

Figure 2. Representative images of microscopic HT29 tumors. *A, left,* fluorescence overlay image [pimonidazole (*green*), Hoechst 33342 (*blue*), and CA9 (*red*)] of a section containing a variety of large and small peritoneal tumors. The series of small tumors <1 mm in dimension situated along a horizontal line through the center of the image all show intense pimonidazole and CA9 fluorescence, suggesting significant hypoxia, with little to no Hoechst 33342 fluorescence. This contrasts with the two larger tumor deposits that extend toward the *top* and *bottom* of the image that show extensive Hoechst 33342 but little pimonidazole or CA9 fluorescence. *Right,* contiguous section stained for CD31. It can be seen that the small tumors that seem hypoxic are essentially avascular, whereas the large tumors have extensive vasculature. *Bar*, 400 μm. *B, left,* fluorescence overlay image [pimonidazole (*green*), Hoechst 33342 (*blue*), and BrdUrd (*red*)] of a section containing a mixture of small peritoneal tumors of various sizes together with stromal elements. Three small deposits with dimensions of ~500 μm (*right*) all show intense central pimonidazole fluorescence with little to no Hoechst 33342 implying significant hypoxia and low perfusion. BrdUrd fluorescence indicating cellular proliferation is seen only in the nonhypoxic rim and is not present in the hypoxic core. *Right,* identical section stained with H&E provided for reference with small tumor deposits indicated. *Bar*, 400 μm. *C, left,* fluorescence overlay image [pimonidazole (*green*), Hoechst 33342 (*blue*), and CA9 (*red*)] of a section containing i.d. tumors. The smaller tumor (*right*) consists of three distinct nodules, each centrally hypoxic with varying degrees of necrosis, separated by highly perfused zones. The larger tumor (*left*) seems minimally hypoxic with widespread perfusion throughout. *Right,* contiguous section stained for CD31. The hypoxic tumor nodules seem essentially avascular, whereas significant vascularity is seen in the well-perfused stromal elements, between nodules. The larger nonhypoxic tumor has extensive vasculature. *Bar*, 400 μm. *D, left,* fluorescence overlay image [pimonidazole (*green*) and CA9 (*red*)] of a section containing a collection of HT29 ascites tumors. Widespread intense staining is observed for both pimonidazole and CA9 implying significant hypoxia. *Right,* identical section stained with H&E provided for reference. *Bar*, 400 μm.

varying size. Of these, the effects of carbogen breathing were examined in five animals each for HT29 and HCT-8. HT29 ascites tumors were harvested from seven animals. (*c*) Hypoxia in i.d. tumors was studied in four animals each for HT29 and HCT-8 with four injection sites per animal.

Results

Hypoxia in macroscopic s.c. tumors. The distribution of regions staining positive for pimonidazole and, for HT29 tumors, CA9 was examined in conjunction with tumor blood perfusion (Hoechst 33342) and morphology (H&E; Fig. 1*A*; Supplementary Fig. S1*A*–*F*). Tumor masses measured after excision were similar [i.e., 467 ± 62 mg (HT29, $n = 5$) and 443 ± 81 mg (HCT-8, $n = 5$)]. Both tumor types displayed similar patterns of pimonidazole binding, the marker being primarily confined to perinecrotic regions with little positivity in regions of frank necrosis. There was a tendency for intratumoral regions staining positive for pimonidazole or for Hoechst 33342 to be mutually exclusive. This was corroborated by a numerical analysis of the spatial correspondence between fluorescence intensities (Fig. 1*B*), which indicated an inverse relationship between Hoechst 33342 and pimonidazole. In contrast, CA9 (in HT29 tumors) generally colocated with pimonidazole though displaying greater extension in the direction of perfused areas. The positive relationship apparent in the spatial correspondence scattergram indicated that pimonidazole and CA9 fluorescence intensity tended to track together. The degree of mismatch between pimonidazole and CA9 was quantified as described in Materials and Methods. It was found that the maximum mismatch occurred at a threshold of 10% of maximum fluorescence intensity and amounted to 37% of grid squares. Of this value, 32% represented grid squares that were positive for CA9 and negative for pimonidazole, whereas 5% were positive for pimonidazole and negative for CA9.

Hypoxia in microscopic peritoneal tumors. Disseminated peritoneal disease developed after i.p. inoculation of tumor cells. Disease progression was significantly slower for HT29 (animal sacrifice required 6–7 weeks after tumor cell inoculation) than for HCT-8 (sacrifice required at 3–4 weeks after inoculation). However, at the time of assay, the gross appearance of peritoneal disease was similar for both cell lines, consisting of a distribution of small tumors adhering to the intestinal serosa. Tumor sizes ranged from a few hundred microns to several millimeters in diameter.

Microscopic examination of peritoneal tumor sections indicated a characteristic relationship between the pattern of hypoxia and tumor size. In general, the smallest tumor deposits (less than ~1 mm diameter) showed intense pimonidazole staining coupled with low Hoechst 33342 staining (Fig. 2*A*; Supplementary Fig. S2*A*). This observation was indicative of hypoxic and relatively poorly perfused tumors. Larger tumors (~1–4 mm diameter) seemed relatively well perfused with generally low levels of pimonidazole staining. In HT29 tumors, the patterns of pimonidazole and CA9 positivity were similar. Anti-CD31 staining (Fig. 2*A*; Supplementary Fig. S2*B*) showed a contrast in vascularity between tumors of different size with the smallest tumors possessing little to no vasculature, whereas larger tumors were well vascularized.

BrdUrd staining indicated that cellular proliferation tended to occur in the rim but not the interior of small avascular tumors (Fig. 2*B*), whereas it was prevalent throughout larger tumors (Supplementary Fig. S2*C* and *D*).

Hypoxia in microscopic i.d. tumors. The patterns of hypoxia in i.d. tumors ranging from a few hundred microns to several millimeters in diameter were examined. Smaller i.d. tumors (<1 mm in diameter) were characterized by a high level of pimonidazole positivity and little to no visible Hoechst 33342 or CD31 positivity (Fig. 2*C*; Supplementary Fig. S2*E* and *F*). In HT29 tumors, positive CA9 staining colocalized with pimonidazole. It was also observed that small i.d. tumors generally contained significant central necrosis. In contrast, for larger i.d. tumors (~1–4 mm in diameter), pimonidazole staining seemed less intense, and Hoechst 33342 was present throughout, together with significant vascularity and minimal necrosis.

Hypoxia in HT29 ascites tumors. On microscopic examination, HT29 ascites tumors appeared similar to small avascular HT29 peritoneal tumors of <1 mm in diameter (Fig. 2*D*). Ascites tumors stained intensely positive for pimonidazole and CA9 but negative for Hoechst 33342, indicating that they were mostly hypoxic with little to no blood perfusion.

Relationship between hypoxia and tumor size. The PPF, as described in Materials and Methods, was estimated for a range of nonascites HT29 tumors of various sizes. For this purpose, the threshold for pimonidazole positivity was taken to be the value of green fluorescence intensity that resulted in a PPF of 0.5% within control regions. PPF estimates for s.c. ($n = 5$), peritoneal ($n = 20$), and i.d. tumors ($n = 14$) are displayed in Fig. 3. This reveals an interesting size dependency of tumor hypoxia. For the smallest peritoneal and i.d. tumors, PPF was very high, approaching ~90% in tumors of several hundred microns diameter. At these sizes, tumors were relatively avascular. As peritoneal and i.d. tumors increased in size, the PPF decreased until in the diameter range ~1 to 4 mm there was little to no positive pimonidazole staining, indicating little to no tumor hypoxia, coupled with the appearance of tumor vascularization and significant blood perfusion. As tumor size increased further into the diameter range equal or greater to ~4 mm, positive pimonidazole staining reappeared in a characteristically perinecrotic distribution pattern that was inversely correlated (see Fig. 1*B*) with Hoechst 33342–defined perfusion.

The effect of carbogen breathing on peritoneal and ascites tumors. The effect of carbogen breathing on hypoxia was studied in HT29 and HCT-8 tumors in the peritoneal cavity. For this

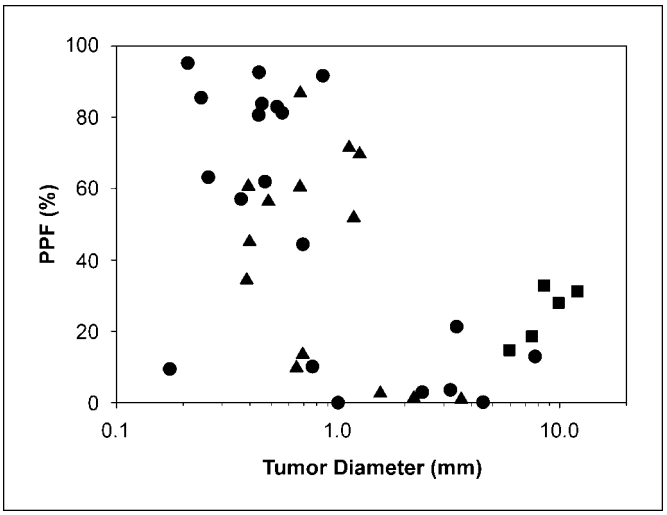

Figure 3. Scatterplot showing the relationship between tumor size and PPF for HT29 tumors. *X-axis,* effective tumor diameter (*D*) derived from the cross-sectional area (*A*) of H&E images according to $D = 2\sqrt{A/\pi}$. ●, peritoneal; ▲, i.d.; ■, s.c.

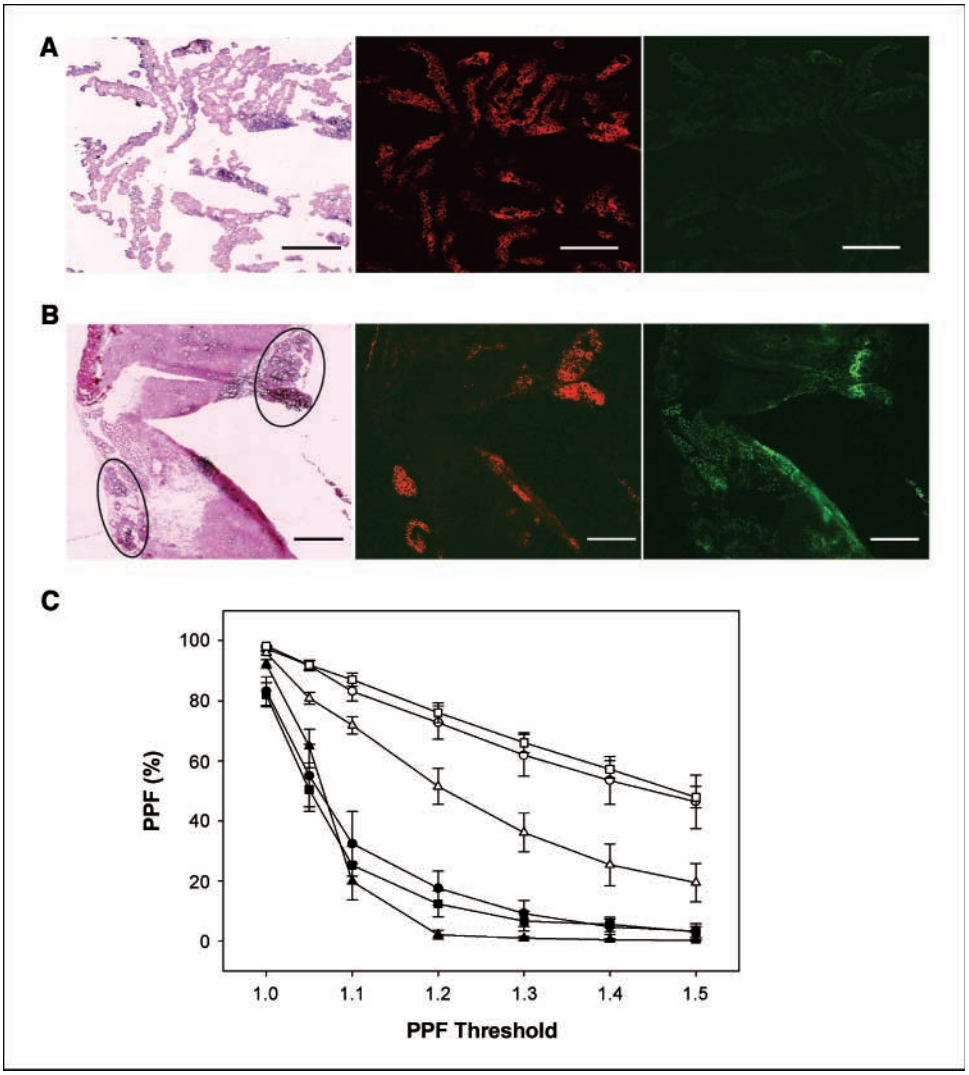

Figure 4. Effect of carbogen breathing on hypoxia in peritoneal tumors. *A,* section containing a collection of HT29 ascites tumors from a carbogen-breathing host. *Left to right,* H&E-stained reference image; fluorescence image showing intense CA9 (*red*) staining; and fluorescence image showing very weak pimonidazole (*green*) staining. *Bar*, 800 μm. *B,* section containing several microscopic HT29 peritoneal tumors from a carbogen-breathing host and associated stromal elements. *Left to right,* H&E-stained reference image with four microscopic tumors indicated (each of the drawn regions contains two microscopic tumors); fluorescence image showing intense CA9 (*red*) staining in all microscopic tumor deposits; and fluorescence image showing weak pimonidazole (*green*) staining in two microscopic deposits (*bottom left*), whereas the others (*top right*) contain regions of intense pimonidazole staining. *Bar*, 800 μm. *C,* PPF as a function of pimonidazole positivity threshold for tumors <1 mm diameter in animals breathing air or carbogen. *Points,* mean of 10 randomly selected tumors; *bars,* 95% CIs. *Closed symbols,* carbogen breathing; *open symbols,* air breathing. ●, HT29 peritoneal tumors; ▲, HT29 ascites, tumors; ■, HCT-8 peritoneal tumors.

purpose, the HT29 model had the advantage that a comparison could be made between the distributions of regions staining positive for CA9 and pimonidazole. As the protein lifetime of CA9 is relatively long (22), its expression was taken to reflect the pre-carbogen hypoxic status, whereas the post-carbogen hypoxic status was indicated by pimonidazole staining. Pilot studies in this system using immunohistochemical staining found that the expression of CA9 was stable *in vivo* for at least 6 h following carbogen breathing (data not shown). In air-breathing conditions, peritoneal and ascites tumors of <1 mm diameter were strongly positive for both pimonidazole and CA9 (Fig. 2*A* and *D*). Following 2 h of carbogen breathing (1 h before and 1 h after pimonidazole administration), there was a reduction in pimonidazole immunofluorescence relative to that of CA9 for both ascites and peritoneal tumors (Fig. 4*A* and *B*). As can be seen in Fig. 4*B*, carbogen breathing did not reduce pimonidazole binding equally in all microscopic tumors, some regions of which seemed refractory to reoxygenation; however, the overall trend was for reduction. Figure 4*C* shows a set of graphs of PPF as a function of pimonidazole positivity threshold (1× to 1.5× the mean fluorescent intensity in control regions) for HT29 peritoneal and ascites tumors and HCT-8 peritoneal tumors. A total of 10 randomly selected tumors of <1 mm diameter were used in each case. This shows that carbogen breathing reduced pimonidazole uptake and, by inference, tumor hypoxia, in a broad range of microscopic i.p. tumors.

Discussion

The objective of this study was to examine the patterns of hypoxia within microscopic tumors grown in experimental animals. This was primarily determined by visualizing the distribution of the exogenously administered hypoxic cell marker pimonidazole with corroboration provided by comparison with the distributions of the hypoxia-regulated protein CA9, tumor blood perfusion, tumor vasculature, and cellular proliferation. In all cases, a consistent relationship was observed between the various indicators studied. In the HT29 system where CA9 could be effectively visualized, the spatial distributions of pimonidazole and CA9 were similar although not identical. The majority of the discrepancies were consistent with known differences between the pO_2 dependency of 2-nitroimidazole binding and hypoxia-inducible factor-1 (HIF-1)/CA9 protein expression (23–26). In particular, CA9 expression extended further than pimonidazole binding toward regions of higher perfusion and presumably higher pO_2 levels.

Regions of positive pimonidazole staining were associated with reduced levels of blood perfusion, vascular density, and cellular proliferation.

In general, it was observed that the degree of tumor hypoxia was dependent on tumor size. Tumors of a few hundred microns diameter were severely hypoxic as gauged by high levels of pimonidazole binding and (for HT29) CA9 expression. These smaller tumors typically displayed little to no blood perfusion or vascularity. As tumors increased in size, they developed a vasculature supply, displayed increased blood perfusion, and became less hypoxic. Tumors between ~1 and ~4 mm in diameter showed little pimonidazole binding and seemed well vascularized. As tumors increased in size beyond this level, the typical pattern of macroscopic tumor hypoxia reappeared, characterized by perinecrotic pimonidazole binding with, in HT29, a broadly similar pattern of CA9 expression.

In human patients, the development of peritoneal metastases is a common occurrence in ovarian and colorectal cancer. Current advances in treatment modalities include locoregional administration of chemotherapeutic agents (27, 28) or radiopharmaceuticals (29, 30) given alone or in combination with other agents. If the patterns of tumor hypoxia observed in the present animal study are replicated in human patients, then the therapeutic efficacy of i.p. treatments could be compromised. Of interest, we also observed that not only tumors in the intestinal serosa but also free-floating avascular tumors in ascites fluid were severely hypoxic and could also be resistant to i.p. therapies.

Animal models of disseminated peritoneal disease may be useful tools in the preclinical evaluation of i.p. therapies. However, given the multiplicity of tumors present and their variability (in terms of size and hypoxic status), the ability to examine the relationship between treatment and response is limited. As individual tumors cannot be monitored on an individual basis, the effects of size-dependent tumor hypoxia cannot be assessed in any but the broadest terms. For this reason, it would be useful to have available models of hypoxia in microscopic tumors that enable monitoring of the response of individual foci to treatment. It was found that microscopic i.d. tumors displayed a similar set of characteristics to peritoneal tumors in terms of the relationship between hypoxia and tumor size. However, the time to development of measurable lesions was very much faster for i.d. tumors. Apparently, this relatively accelerated development reflects the enhanced vascularity of the dermis and its ability to support tumor angiogenesis. Certainly, within only a few days of cell inoculation, larger i.d. tumors seemed well vascularized. If, as seems the case, microscopic i.d. tumors are similar to peritoneal disease in terms of the size dependency of tumor hypoxia, then they may provide a useful model system to study the effects of tumor hypoxia on therapeutic intervention.

To associate a numerical value with the level of tumor hypoxia in sections, we used the PPF. This corresponds to the fraction of viable tumor area with a pimonidazole immunofluorescent intensity greater than a threshold value derived from control regions on the same slide. The extent of pimonidazole positivity, and thus the numerical value of PPF, is dependent on the selected threshold. This can be seen in Fig. 4*C*, where threshold values were used ranging from 1× to 1.5× the mean fluorescent intensity in control regions. As the PPF is threshold dependent, we do not ascribe any direct physical significance to its numerical value. Its primary utility is as a metric, defined in a consistent manner for any given experiment, which enables tumors to be compared. Using PPF, we could visualize the relationship between tumor hypoxia and tumor size (Fig. 3) or that carbogen breathing tended to reduce tumor hypoxia (Fig. 4*C*). Although theoretically, it may be possible by comparing estimates of radiobiological hypoxic fraction with PPF to derive a "radiobiologically correct" threshold, the evaluation of clonogenic surviving fraction for microscopic tumors presents significant practical difficulties.

Tumor hypoxia and angiogenesis are intimately related (31–33) with the hypoxia-regulated transcription factor HIF-1 driving the expression of a host of proangiogenic proteins (34). Our results using two different tumor cell lines in both peritoneal and i.d. sites suggest the possibility that the existence of severe hypoxia in microscopic tumors is common irrespective of cell line and tumor location and reflects the preangiogenic stage of tumor development. If the earliest stages of metastatic developmental in human patients follow a similar pattern, the majority of these microscopic tumors will be hypoxic and thus resistant to ionizing radiation and several chemotherapeutic agents. Clinical and preclinical studies on radiotherapy given in combination with hypoxia modulating agents have shown some promising results in macroscopic tumors (35–39). The present study indicates that carbogen breathing significantly decreased hypoxia in avascular microscopic tumors. This and possibly other hypoxia-modulating agents may also have a role in the treatment of micrometastatic disease.

Acknowledgments

Received 11/28/2006; revised 6/13/2007; accepted 6/20/2007.

Grant support: NIH grants R01 CA84596 and R24 CA83084.

The costs of publication of this article were defrayed in part by the payment of page charges. This article must therefore be hereby marked *advertisement* in accordance with 18 U.S.C. Section 1734 solely to indicate this fact.

References

1. Wouters BG, Weppler SA, Koritzinsky M, et al. Hypoxia as a target for combined modality treatments. Eur J Cancer 2002;38:240–57.
2. Goethals L, Debucquoy A, Perneel C, et al. Hypoxia in human colorectal adenocarcinoma: comparison between extrinsic and potential intrinsic hypoxia markers. Int J Radiat Oncol Biol Phys 2006; 65:246–54.
3. Brizel DM, Sibley GS, Prosnitz LR, Scher RL, Dewhirst MW. Tumor hypoxia adversely affects the prognosis of carcinoma of the head and neck. Int J Radiat Oncol Biol Phys 1997;38:285–9.
4. Nordsmark M, Overgaard M, Overgaard J. Pretreatment oxygenation predicts radiation response in advanced squamous cell carcinoma of the head and neck. Radiother Oncol 1996;41:31–9.
5. Vaupel P, Schlenger K, Knoop C, Hockel M. Oxygenation of human tumors—evaluation of tissue oxygen distribution in breast cancers by computerized O_2 tension measurements. Cancer Res 1991;51:3316–22.
6. Teicher BA. Hypoxia and drug-resistance. Cancer Metastasis Rev 1994;13:139–68.
7. Shannon AM, Bouchier-Hayes DJ, Condron CM, Toomey D. Tumour hypoxia, chemotherapeutic resistance, and hypoxia-related therapies. Cancer Treat Rev 2003;29:297–307.
8. Le QT, Sutphin PD, Raychaudhuri S, et al. Identification of osteopontin as a prognostic plasma marker for head and neck squamous cell carcinomas. Clin Cancer Res 2003;9:59–67.
9. Overgaard J, Eriksen JG, Nordsmark M, Alsner J, Horsman MR. Plasma osteopontin, hypoxia, and response to the hypoxia sensitiser nimorazole in radiotherapy of head and neck cancer: results from the DAHANCA 5 randomised double-blind placebo-controlled trial. Lancet Oncol 2005;6:757–64.
10. Zhao DW, Constantinescu A, Hahn EW, Mason RP. Tumor oxygen dynamics with respect to growth and respiratory challenge: investigation of the Dunning prostate R3327-HI tumor. Radiat Res 2001; 156:510–20.
11. De Jaeger K, Merlo FM, Kavanagh MC, Fyles AW, Hedley D, Hill RP. Heterogeneity of tumor oxygenation: relationship to tumor necrosis, tumor size, and metastasis. Int J Radiat Oncol Biol Phys 1998;42:717–21.
12. Milross CG, Tucker SL, Mason KA, Hunter NR, Milas

L. The effect of tumor size on necrosis and polarographically measured pO(2). Acta Oncol 1997;36:183–9.
13. Raleigh JA, Chou SC, Arteel GE, Horsman MR. Comparisons among pimonidazole binding, oxygen electrode measurements, and radiation response in C3H mouse tumors. Radiat Res 1999;151:580–9.
14. Kaanders J, Wijffels K, Marres HAM, et al. Pimonidazole binding and tumor vascularity predict for treatment outcome in head and neck cancer. Cancer Res 2002;62:7066–74.
15. Raleigh JA, Calkins-Adams DP, Rinker LH, et al. Hypoxia and vascular endothelial growth factor expression in human squamous cell carcinomas using pimonidazole as a hypoxia marker. Cancer Res 1998; 58:3765–8.
16. Driessen A, Landuyt W, Pastorekova S, et al. Expression of carbonic anhydrase IX (CA IX), a hypoxia-related protein, rather than vascular-endothelial growth factor (VEGF), a pro-angiogenic factor, correlates with an extremely poor prognosis in esophageal and gastric adenocarcinomas. Ann Surg 2006;243:334–40.
17. Hoskin PJ, Sibtain A, Daley FM, Wilson GD. GLUTI and CAIX as intrinsic markers of hypoxia in bladder cancer: relationship with vascularity and proliferation as predictors of outcome of ARCON. Br J Cancer 2003;89: 1290–7.
18. Potter CPS, Harris AL. Diagnostic, prognostic, and therapeutic implications of carbonic anhydrases in cancer. Br J Cancer 2003;89:2–7.
19. Koukourakis MI, Giatromanolaki A, Sivridis E, et al. Hypoxia-regulated carbonic anhydrase-9 (CA9) relates to poor vascularization and resistance of squamous cell head and neck cancer to chemoradiotherapy. Clin Cancer Res 2001;7:3399–403.
20. Beasley NJP, Wykoff CC, Watson PH, et al. Carbonic anhydrase IX, an endogenous hypoxia marker, expression in head and neck squamous cell carcinoma and its relationship to hypoxia, necrosis, and microvessel density. Cancer Res 2001;61:5262–7.
21. Chrastina A, Zavada J, Parkkila S, et al. Biodistribution and pharmacokinetics of I-125-labeled monoclonal antibody M75 specific for carbonic anhydrase IX, an intrinsic marker of hypoxia, in nude mice xenografted with human colorectal carcinoma. Int J Cancer 2003;105: 873–81.
22. Vordermark D, Kaffer A, Riedl S, Katzer A, Flentje M. Characterization of carbonic anhydrase IX (CA IX) as an endogenous marker of chronic hypoxia in live human tumor cells. Int J Radiat Oncol Biol Phys 2005; 61:1197–207.
23. Gross MW, Karbach U, Groebe K, Franko AJ, Muellerklieser W. Calibration of misonidazole labeling by simultaneous measurement of oxygen-tension and labeling density in multicellular spheroids. Int J Cancer 1995;61:567–73.
24. Schneider RF, Engelhardt EL, Stobbe CC, Fenning MC, Chapman JD. The synthesis and radiolabeling of novel markers of tissue hypoxia of the iodinated azomycin nucleoside class. J Labeled Compounds Radiopharm 1997;39:541–57.
25. Jiang BH, Semenza GL, Bauer C, Marti HH. Hypoxia-inducible factor 1 levels vary exponentially over a physiologically relevant range of O-2 tension. Am J Physiol Cell Physiol 1996;40:C1172–80.
26. Sorensen BS, Hao J, Overgaard J, et al. Influence of oxygen concentration and pH on expression of hypoxia induced genes. Radiother Oncol 2005;76:187–93.
27. Yan TD, Black D, Savady R, Sugarbaker PH. Systematic review on the efficacy of cytoreductive surgery combined with perioperative intraperitoneal chemotherapy for peritoneal carcinomatosis from colorectal carcinoma. J Clin Oncol 2006;24:4011–9.
28. Muggia F, Kosloff R. Investigational agents for epithelial ovarian cancer. Expert Rev Anticancer Ther 2005;5:855–68.
29. Verheijen RH, Massuger LF, Benigno BB, et al. Phase III trial of intraperitoneal therapy with yttrium-90-labeled HMFG1 murine monoclonal antibody in patients with epithelial ovarian cancer after a surgically defined complete remission. J Clin Oncol 2006;24:571–8.
30. Alvarez RD, Huh WK, Khazaeli MB, et al. A phase I study of combined modality (90)Yttrium-CC49 intraperitoneal radioimmunotherapy for ovarian cancer. Clin Cancer Res 2002;8:2806–11.
31. Pugh CW, Ratcliffe PJ. Regulation of angiogenesis by hypoxia: role of the HIF system. Nat Med 2003;9:677–84.
32. Hirota K, Semenza GL. Regulation of angiogenesis by hypoxia-inducible factor 1. Crit Rev Oncol Hematol 2006;59:15–26.
33. Jain RK. Normalization of tumor vasculature: an emerging concept in antiangiogenic therapy. Science 2005;307:58–62.
34. Harris AL. Hypoxia—a key regulatory factor in tumour growth. Nat Rev Cancer 2002;2:38–47.
35. Kaanders J, Pop LAM, Marres HAM, et al. Accelerated radiotherapy with carbogen and nicotinamide (ARCON) for laryngeal cancer. Radiother Oncol 1998;48:115–22.
36. Bernier J, Denekamp J, Rojas A, et al. ARCON: accelerated radiotherapy with carbogen and nicotinamide in head and neck squamous cell carcinomas. The experience of the Cooperative Group of Radiotherapy of the European Organization for Research and Treatment of Cancer (EORTC). Radiother Oncol 2000;55:111–9.
37. van Laarhoven HWM, Bussink J, Lok J, et al. Modulation of hypoxia in murine liver metastases of colon carcinoma by nicotinamide and carbogen. Radiat Res 2005;164:245–9.
38. van Laarhoven HWM, Bussink J, Lok J, Punt CJA, Heerschap A, van der Kogel AJ. Effects of nicotinamide and carbogen in different murine colon carcinomas: Immunohistochemical analysis of vascular architecture and microenvironmental parameters. Int J Radiat Oncol Biol Phys 2004;60:310–21.
39. Kaanders J, Bussink J, van der Kogel AJ. ARCON: a novel biology-based approach in radiotherapy. Lancet Oncol 2002;3:728–37.

Visualization of Hypoxia in Microscopic Tumors by Immunofluorescent Microscopy

Xiao-Feng Li, Sean Carlin, Muneyasu Urano, et al.

Cancer Res 2007;67:7646-7653.